Dynamic modeling and simulation of a pressurized alkaline water electrolyzer: a multiphysics approach

Alvaro Iribarren
Dept. of Electrical, Electronic and Communications Engineering
Public University of Navarre
Campus de Arrosadía
31006 Pamplona, Spain
alvaro.iribarren@unavarra.es

Ernesto Barrios
Dept. of Electrical, Electronic and Communications Engineering
Public University of Navarre
Campus de Arrosadía
31006 Pamplona, Spain
ernesto.barrios@unavarra.es

Harkaitz Ibaiondo
Ingeteam Power Technology
Zamudio, Spain
Harkaitz.Ibaiondo@ingeteam.com

Alain Sanchez-Ruiz
Ingeteam R&D Europe
Zamudio, Spain
Alain.Sanchez@ingeteam.com

Joseba Arza
Ingeteam R&D Europe
Zamudio, Spain
joseba.arza@ingeteam.com

Pablo Sanchis
Institute of Smart Cities
Detp. of Electrical, Electronic and Communications Engineering
Public University of Navarre
Campus de Arrosadia
31006 Pamplona, Spain
pablo.sanchis@unavarra.es

Alfredo Ursúa
Institute of Smart Cities
Dept. of Electrical, Electronic and Communications Engineering
Public University of Navarre
Campus de Arrosadia
31006 Pamplona, Spain
alfredo.ursua@unavarra.es

***Abstract*—In this paper a dynamic model for the simulation of pressurized alkaline water electrolyzers is presented. The model has been developed following a multiphysics approach, integrating electrochemical, thermodynamic, heat transfer and gas evolution processes in order to faithfully reproduce the complete dynamical behavior of these systems. The model has been implemented on MATLAB/Simulink and validated through experimental data from a 1 Nm^3h^{-1} commercial alkaline water electrolyzer, and the simulated results have been found to be consistent with the real measured values. This model has a great potential to predict the behavior of alkaline water electrolyzers coupled with renewable energy sources, making it a very useful tool for designing efficient green hydrogen production systems.**

Keywords—alkaline water electrolyzer, green hydrogen production, dynamic modeling, renewable energy.

I. INTRODUCTION

Over the last few years, interest in renewable hydrogen production has increased largely. This element is expected to play a pivotal role in the transition that the world is already undergoing towards a cleaner and more environmentally friendly place. Hydrogen is not a primary energy source, but an energy carrier capable of storing energy and delivering it whenever is needed. Green hydrogen (i.e., hydrogen produced from renewable energy) has a great potential because it links renewable electricity with a range of end-use applications where direct electrification is not feasible.

Industry is the sector where green hydrogen has a more direct application, as it is an essential chemical agent for the production of ammonia, methanol, petroleum products, polymers and many other materials and products [1]. The energy sector constitutes another application where green hydrogen can play a key role, mainly due to the need to solve problems related to the characteristic fluctuations produced in renewable sources such as wind or solar. Its high energy density, long-term storability and transportability makes of hydrogen production an attractive solution, especially for inter-seasonal storage [2]. Moreover, there is a growing concern about pollution in the transport sector. Along with the development of battery-based electric vehicles, hydrogen-based vehicles are an interesting alternative for eliminating pollution. Particularly, green hydrogen seems to be most appropriate for decarbonizing heavy vehicles, trains, ships, and airplanes, where the use of batteries would not be suitable due to their excessive weight [3].

The union of all these sectors based on hydrogen as the predominant energy vector generates what nowadays is disclosed as hydrogen economy. In order for this hydrogen economy to be completely carbon-free, hydrogen must be produced using non-polluting energy sources, which is achieved mainly through the electrolysis of water using renewable electricity. This is why interest in water electrolysis technologies has increased largely over the past years [4].

There are various water electrolysis technologies commercially available, which differ in the type of electrolyte used: alkaline electrolysis cells (AEC), proton exchange membrane electrolysis cells (PEMEC), solid oxide electrolysis cells (SOEC) and anion exchange membrane electrolysis cells (AEMEC). From these, AEC is nowadays the most mature and widespread used for large-scale industrial applications [5]. Although its maturity, there remain some aspects that are still unstudied about AEC, especially those related to a fluctuating electrical input, a key aspect to consider when the electrolyzer is designed to operate with renewable sources. This is why the dynamic modeling of electrolysis systems has uttermost importance in understanding the operational behavior of the electrolyzer coupled with renewable energy sources.

Many mathematical models exist in literature for characterizing AEC. Ulleberg [6] developed a semi-empirical model for the representation of the static electrical behavior of an alkaline electrolyzer, and also proposed a dynamic thermal model for the calculation of the overall cell temperature. Ursúa et al. [7] were able to predict the dynamic electrical response of a pressurized alkaline electrolyzer with high accuracy, and Diéguez et al. [8] developed the thermal model for the same electrolyzer. Another approach was published by Haug et al. [9] who developed a model based on classical process engineering for the prediction of the product gas purity in alkaline water electrolysis.

This work has been supported by the Spanish State Research Agency (AEI/10.13039/501100011033) under grants PID2019-111262RB-I00 and PID2019-110956RB-I00, and by Ingeteam R&D Europe.

The majority of the models rely on a single-physics approach and only represent one aspect about the operational behavior of the electrolysis system, be it its electrical, thermal or gas production capacity. Furthermore, most of them lack a comprehensive analysis of the dynamic response, which is crucial for the operation with renewable sources.

In this study, a dynamic model for a pressurized AEC system is developed following a multiphysics approach, integrating various submodels in order to achieve a detailed characterization of the different phenomena that occur in the electrolyzer. The modeling and simulation has been performed using MATLAB/Simulink and results have been validated through experimental data from a 1 Nm^3h^{-1} commercial alkaline water electrolyzer. The contribution is organized as follows. Section II describes the electrical submodel. Section III presents the thermal submodel. Section IV shows the gas generation and product gas purity submodel. In Section V, the integrated complete model is validated through a comparison of experimental and simulated results. Finally, in Section VI the main conclusions are summed up.

II. Electrical Submodel

The decomposition of water into hydrogen and oxygen can be achieved when a minimum electrical voltage is applied between two electrodes separated by an electrolyte with good ionic conductivity. In the case of AEC, the electrolyte is usually an aqueous solution of potassium hydroxide (KOH) at 25 – 30 wt% in order to maximize its ionic conductivity. The total reaction of water electrolysis is (1), whereas (2) and (3) are the cathodic and anodic half-reactions, respectively:

$$H_2O\ (l) \rightarrow H_2(g) + \frac{1}{2}O_2(g) \quad (1)$$

$$2H_2O\ (l) + 2e^- \rightarrow H_2(g) + 2OH^-(aq.) \quad (2)$$

$$2OH^-(aq.) \rightarrow H_2O(l) + \frac{1}{2}O_2(g) + 2e^- \quad (3)$$

The energy required for the electrolysis to take place at a given temperature (T) and pressure (P) is determined by the enthalpy change of the process (ΔH), which is equal to the sum of the Gibbs energy change (ΔG) and the temperature times the entropy change (ΔS). This relationship is expressed in (4):

$$\Delta H = \Delta G + T\Delta S \quad (4)$$

The minimum electrical energy to start the water electrolysis is given by the variation of the Gibbs energy, as the rest corresponds to thermal energy. This minimum voltage associated to the Gibbs free energy is the so-called reversible potential (V_{rev}), and can be calculated as in (5) using Faraday's law of electrolysis:

$$V_{rev} = \Delta G / zF \quad (5)$$

where z is the number of electrons transferred per hydrogen molecule ($z = 2$) and F is the Faraday's constant (96,485 C/mol).

Ideally, the cell voltage is equal to V_{rev}, but due the presence of irreversibilities the actual working potential is always higher, resulting in a loss of efficiency. Such irreversibilities consist of overvoltages caused mainly by ohmic losses (V_{ohm}), activation losses (V_{act}) and diffusion losses (V_{diff}). Thus, the cell potential (V_{cell}) can be written as:

$$V_{cell} = V_{rev} + V_{ohm} + V_{act} + V_{diff} \quad (6)$$

If the electrolyzer presents a bipolar configuration with N_s cells connected in series, the overall voltage of the stack (V_E) is equal to:

$$V_E = N_s\left(V_{rev} + V_{ohm} + V_{act} + V_{diff}\right) \quad (7)$$

Fig. 1 shows the electrical submodel implemented in MATLAB/Simulink, where the different electrical phenomena are represented using Simscape blocks from the Electrical Foundation Library. Most of these components are variable elements or controlled sources whose actual value is computed in auxiliary blocks in which physical and empirical equations are constructed.

The reversible voltage can be modeled as a voltage source that depends on the operating temperature and pressure. V_{rev} is equal to 1.229 V at standard conditions (25 ºC, 1 atm), but this value decreases as temperature rises, or slightly increases as pressure rises. The temperature and pressure dependance of V_{rev} can be derived from Nernst equation (8):

$$V_{rev} = V^0_{rev,T}(T) + \frac{RT}{zF} ln\left[\frac{(P-P_{v,KOH})(P-P_{v,KOH})^2}{a_{H_2O,KOH}}\right] \quad (8)$$

where $V^0_{rev,T}$ is the reversible voltage at standard pressure (1 atm) as a function of temperature, R is the universal gas constant (8.314 J mol^{-1} K^{-1}), $P_{v,KOH}$ is the vapor pressure of the electrolytic solution and $a_{H_2O,KOH}$ is the water activity in the electrolyte. Empirical expressions for $V^0_{rev,T}$, $P_{v,KOH}$ and $a_{H_2O,KOH}$ can be found in [7].

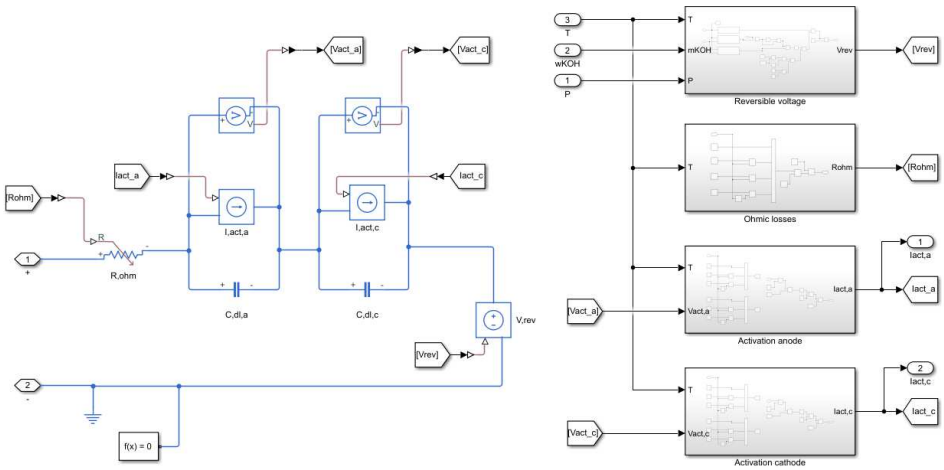

Fig. 1. Electrical submodel implemented in Simulink.

The overvoltage V_{ohm} corresponds to the ohmic losses associated to the resistance to the flow of electrical charges (electrons and ions) across the cell. The value of this overvoltage increases linearly with the current passing through the electrolysis cell (I) following Ohm's law (9):

$$V_{ohm} = I\,R_{ohm} \tag{9}$$

The dynamic response of V_{ohm} is practically instantaneous against changes in the electrolyzer input current or voltage, thus it can be modeled with an ohmic resistance R_{ohm} which can be expressed as:

$$R_{ohm} = \frac{r}{A} \tag{10}$$

where r is the area-specific resistance of the cell and A is the electrode area. Also, the value of R_{ohm} depends on the operating temperature, therefore a variable resistor is employed in the model and the following expression for r is used:

$$r = r_1 + r_2 T + \frac{r_3}{T} + \frac{r_4}{T^2} \tag{11}$$

where r_1, r_2, r_3 and r_4 are parameters to be adjusted based on experimental data of the electrolyzer. r_2 models the increment of the electronic resistance with temperature, whereas r_3 and r_4 model the reduction of the ionic resistance of the electrolyte with temperature. In general, as temperature rises the overall electric resistance of the cell is reduced because the weight of the ionic resistance in R_{ohm} is greater than the electronic one.

The overvoltage V_{act} is caused by the kinetics of the redox reactions that take place in the anode and cathode. In order to start the formation of hydrogen and oxygen an extra energy is required which translates in activation losses. The relationship between the current and the activation overpotential in an electrode is given by the Butler-Volmer equation (12):

$$I = I_0 \left[exp\left(\frac{\alpha z F V_{act}}{RT}\right) - exp\left(-\frac{(1-\alpha) z F V_{act}}{RT}\right)\right] \tag{12}$$

where I_0 is the equilibrium current where the rate of the oxidation reaction is equal to the rate of the reduction reaction, and α is the charge transfer coefficient and takes values between 0 and 1. For high values of the activation potential, the Butler-Volmer equation can be approximated by:

$$V_{act} = \frac{RT}{\alpha z F} ln\left(\frac{I}{I_0}\right) \tag{13}$$

This expression is known as the Tafel equation and is commonly employed to model the I-V_{act} relationship in fuel-cells and electrolyzers. In this study, the activation phenomena is modeled using controlled current sources dependent on their own voltage using a modification of the Tafel equation in order to cover the full current range:

$$I_{act,i} = t_i \left[exp\left(\frac{V_{act,i}}{s_i}\right) - 1\right] \tag{14}$$

where the subscript i refers to either anode or cathode, and parameters s and t are adjusted based on experimental data of the electrolyzer. Also, the activation losses are temperature dependent, therefore the following expressions are used for parameters s and t of each electrode (i):

$$s_i = s_{1,i} + s_{2,i} T + s_{3,i} T^2 \tag{15}$$

$$t_i = t_{1,i} + t_{2,i} T + t_{3,i} T^2 \tag{16}$$

Furthermore, V_{act} presents a dynamic response due to the formation of a double-layer caused by the accumulation of electrical charges with opposite polarity on the surface of the electrodes, acting as a capacitor. In order to reproduce the dynamics of this double-layer effect, a capacitor is placed in parallel with the current source that model the activation phenomena of each electrode.

Finally, the overvoltage V_{diff} is associated to mass transfer phenomena that happen inside the electrochemical cell, mainly the diffusion of species driven by concentration gradients in the proximity of the electrodes, where the concentration of products increases and that of reactants decreases as the redox reactions evolve. V_{diff} only becomes significant when sufficiently high current densities are applied, thus its influence is negligible for alkaline electrolyzers due to their relatively low operating current densities (0.2 – 0.8 A/cm^2). Therefore V_{diff} is not included in this model.

The values of the parameters employed to construct the different electrical components of the model have been empirically determined following the methodology explained in [7].

III. Thermal Submodel

Fig. 2 shows the thermal submodel implemented in MATLAB/Simulink, where the different thermal phenomena are represented using Simscape blocks from the Thermal Foundation Library. As in the electrical submodel, most of the components employed are controlled sources whose actual value is computed in auxiliary blocks in which physical and empirical equations are constructed.

A lumped capacitance method has been used for modeling the time depence of the electrolyzer temperature. This method considers the entire electrolyzer as a single thermal mass, without internal gradients of temperature. As shown in [8] the difference between the temperatures of the main electrolyzer components is usually lower than 10 ºC, therefore this can be considered a reasonable approximation. Following this, the overall thermal energy balance can be expressed as:

$$C_t \frac{dT}{dt} = \dot{Q}_{gen} - \dot{Q}_{loss} - \dot{Q}_{cool} - \dot{Q}_{species} \tag{17}$$

The term on the left-hand side of (17) models the time evolution of the overall electrolyzer temperature, which depends on the lumped thermal capacity C_t (J/K).

$\dot{Q}_{gen}$ corresponds to the internal heat generation, which is the result of the electrical power input dissipated as heat. In most commercial electrolyzers the thermal energy demand of the process, $T\Delta S$, is supplied by electricity, therefore the minimum voltage to start electrolysis is greater than the reversible voltage. This minimum voltage needed is referred to as the thermoneutral voltage (V_{tn}), which in an ideal process is equal to the voltage corresponding to the enthalpy change of the reaction. The enthalpy voltage ($V_{\Delta h}$) can be calculated as in (18) using Faraday's law of electrolysis:

$$V_{\Delta h} = \Delta H / zF \xrightarrow{ideal\ process} V_{\Delta h} = V_{tn} \tag{18}$$

In a real electrolysis process V_{tn} is greater than $V_{\Delta h}$ due to the presence of overvoltages associated to irreversibilities in the thermodynamic process (V_{irrev}), therefore:

$$V_{tn} = V_{\Delta h} + V_{irrev} \tag{19}$$

Considering the formation of water vapor along with the produced hydrogen and oxygen as the main irreversibility of the process, V_{irrev} can be computed as:

$$V_{irrev} = y\frac{\left(h_{H_2O(g),T,P_{v,KOH}} - h^0_{H_2O(l)}\right)}{zF} \quad (20)$$

$$y = \frac{P_{v,KOH}}{P-P_{v,KOH}} + \frac{1}{2}\frac{P_{v,KOH}}{P-P_{v,KOH}} \quad (21)$$

where y corresponds to the number of moles of water vapor produced, both in the cathode and in the anode, per mole of H_2 produced by electrolysis, $h_{H_2O(g),T,P_{v,KOH}}$ is the molar enthalpy of the produced water vapor at the operating temperature and vapor pressure of the electrolyte, and $h^0_{H_2O(l)}$ is the molar enthalpy of liquid water at standard conditions. Values of $V_{\Delta h}$, $h_{H_2O(g),T,P_{v,KOH}}$ and $h^0_{H_2O(l)}$ can be obtained from thermodynamic charts and tables abundant in literature.

The generation of heat occurs when electrical input of the electrolyzer is greater than the thermodynamical energy demand, which translates into a difference between the actual electrolyzer voltage (V_E) and the thermoneutral voltage for the whole stack (N_sV_{tn}). This energy excess, or waste heat, can be computed as:

$$\dot{Q}_{gen} = I(V_E - N_sV_{tn}) \quad (22)$$

The term $\dot{Q}_{loss}$ represents the total heat loss to the ambient due to convection and radiation. In the model, an overall convective-radiative heat transfer coefficient (h) is employed, and only heat transfer processes between the ambient and the stack and gas separators are considered, since they are the electrolyzer components that expose the largest surface areas. According to this, heat losses are evaluated as:

$$\dot{Q}_{loss} = h\left(A_{stack} + A_{sep}\right)(T - T_{amb}) \quad (23)$$

where A_{stack} is the external surface of the cells stack, A_{sep} is the total external surface of both gas separators and T_{amb} is the ambient temperature.

$\dot{Q}_{cool}$ corresponds to the auxiliary cooling power required not to exceed the maximum operating temperature allowed by the electrolyzer manufacturer. Details about the modeling of the removed heat through a refrigeration system with cooling water can be found in [6]. Finally, the term $\dot{Q}_{species}$ is associated to the heat lost due to the species leaving the system (extracted flows of H_2 and O_2) and to the heating of the feed water. This value is considerably inferior to the rest of the terms, so it has not been included in this model [8].

As can be seen in Fig. 2. the electrolyzer is modeled in Simulink using a thermal mass, $\dot{Q}_{gen}$ and $\dot{Q}_{cool}$ are introduced through controlled heat sources, and a convective heat transfer element is used for $\dot{Q}_{loss}$. Parameters such as the lumped thermal capacity (C_t) and the overall convective-radiative heat transfer coefficient (h) have been empirically determined following the methodology explained in [8].

IV. Gas Production Submodel

Molar flow rates of hydrogen and oxygen generated at the electrodes can be related to the activation current at the cathode and anode, respectively, following Faraday's law:

$$\dot{n}_{H_2,gen} = \frac{N_sI_{act,c}}{zF}\eta_F \quad (24)$$

$$\dot{n}_{O_2,gen} = \frac{1}{2}\frac{N_sI_{act,a}}{zF}\eta_F \quad (25)$$

where η_F represents the Faraday efficiency, defined as the ratio between the actual and theoretical produced flow rates, caused by parasitic current losses. In this study, a constant value of 0.95 is assumed for η_F, similar to that established in the scientific literature [10].

Along with these produced gases, water vapor ($H_2O(g)$) is also formed at the electrodes, causing irreversibilities and worsening the efficiency of the process. Considering this water vapor is in equilibrium with the generated gases, molar flow rates of $H_2O(g)$ produced at the cathode and anode can be computed as:

$$\dot{n}_{H_2O(g),gen,c} = \frac{P_{v,KOH}}{P-P_{v,KOH}}\dot{n}_{H_2,gen} \quad (26)$$

$$\dot{n}_{H_2O(g),gen,a} = \frac{P_{v,KOH}}{P-P_{v,KOH}}\dot{n}_{O_2,gen} \quad (27)$$

In addition to the water vapor content, the purity of the generated gases is compromised due to the presence of hydrogen through the oxygen flow (HTO) and of oxygen through the hydrogen flow (OTH). This is caused by two different phenomena: crossover of dissolved gasses through the separator; and species transport through the mixing pipe installed between the anode and cathode gas separators.

In alkaline water electrolysis the separator is a porous diaphragm, typically a Zirfon diaphragm, which prevents short circuits between the electrodes and the mixing of the produced hydrogen and oxygen. Although this separator is impermeable for gases, diffusional crossover of dissolved species in liquid phase occurs due to concentration gradients between cathode and anode. According to Fick's law, the molar flow rates of H_2 and O_2 that diffuse through the separator can be computed as:

$$\dot{n}_{H_2,cross} = \frac{D_{H_2}}{d_{sep}}\frac{\varepsilon_{sep}}{\tau_{sep}}\left(c_{H_2,c} - c_{H_2,a}\right)A_{cell} \quad (28)$$

$$\dot{n}_{O_2,cross} = \frac{D_{O_2}}{d_{sep}}\frac{\varepsilon_{sep}}{\tau_{sep}}\left(c_{O_2,a} - c_{O_2,c}\right)A_{cell} \quad (29)$$

where D_{H_2} and D_{O_2} are the molecular diffusion coefficients of H_2 and O_2 in the electrolyte; d_{sep}, ε_{sep} and τ_{sep} are the separator thickness, porosity, and tortuosity, respectively; A_{cell} is the cell surface; and $c_{H_2,c}$, $c_{H_2,a}$, $c_{O_2,c}$ and $c_{O_2,a}$ are the molar concentrations of H_2 and O_2 in the cathode and anode compartments. Typical values for d_{sep} , ε_{sep} and τ_{sep} corresponding to a Zirfon diaphragm are given in [9], whereas the diffusional coefficients D_{H_2} and D_{O_2} can be found in [11]. Furthermore, AEC systems usually present a mixing pipe, or

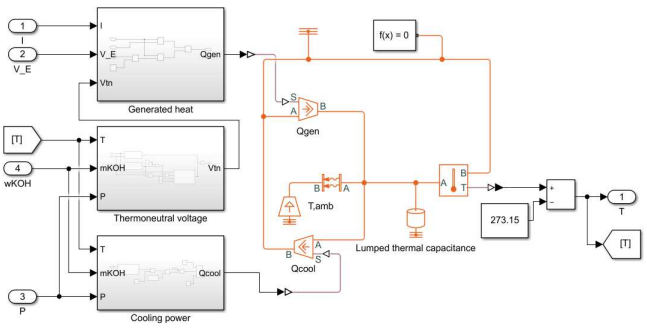

Fig. 2. Thermal submodel implemented in Simulink.

equalization line, installed between the anode and cathode gas separators in order to balance the OH^- charges consumed/produced along with the electrochemical reaction. This mixing pipe increases foreign gas content due to transport of species caused by concentration gradients or differential pressure between both gas separators. Flow rates of H_2 and O_2 that are transported to the opposite separator through the mixing pipe can be written as a fraction of the net flow that enters their respective original separator:

$$\dot{n}_{H_2,mix} = \lambda\left(\dot{n}_{H_2,gen} - \dot{n}_{H_2,cross}\right) \quad (30)$$

$$\dot{n}_{O_2,mix} = \mu\left(\dot{n}_{O_2,gen} - \dot{n}_{O_2,cross}\right) \quad (31)$$

where λ and μ, which present values between 0 and 1, need to be determined experimentally with data from the HTO and OTH sensors of the electrolyzer under study. Considering that water vapor is completely removed thanks to the presence of condenser filters and dryers at the outlet of both gas separators, expressions for HTO and OTH can be written as:

$$HTO = \frac{\dot{n}_{H_2,cross} + \dot{n}_{H_2,mix}}{\dot{n}_{O_2,gen} - \dot{n}_{O_2,cross} - \dot{n}_{O_2,mix} + \dot{n}_{H_2,cross} + \dot{n}_{H_2,mix}} \quad (32)$$

$$OTH = \frac{\dot{n}_{O_2,cross} + \dot{n}_{O_2,mix}}{\dot{n}_{H_2,gen} - \dot{n}_{H_2,cross} - \dot{n}_{H_2,mix} + \dot{n}_{O_2,cross} + \dot{n}_{O_2,mix}} \quad (33)$$

Finally, the usable hydrogen flow that is obtained at the outlet of the electrolysis system is equal to:

$$\dot{n}_{H_2,out} = \dot{n}_{H_2,gen} - \dot{n}_{H_2,cross} - \dot{n}_{H_2,mix} \quad (34)$$

Equations (24) to (34) are implemented in MATLAB/Simulink and this gas production submodel is integrated along with the electrical and thermal submodels, creating the complete multiphysics model, as can be seen in Fig. 3.

V. Model Validation: Comparison of Experimental and Simulated Results

A. Electrical submodel validation

First, the electrical behavior of the electrolyzer operating on a static regime has been analyzed. Fig. 4 shows the experimental and simulated $I-V$ curves of the electrolyzer at a fixed pressure of 25 bar and for three different operating temperatures (15, 35 and 65 ºC). Results demonstrate that the model faithfully predicts the static electrical response of the stack, as the simulated $I-V$ curves reproduce very accurately the experimental ones. As it can be observed, an increase in operating temperature favors the reduction of electricity consumption, as the stack voltage is reduced for the same

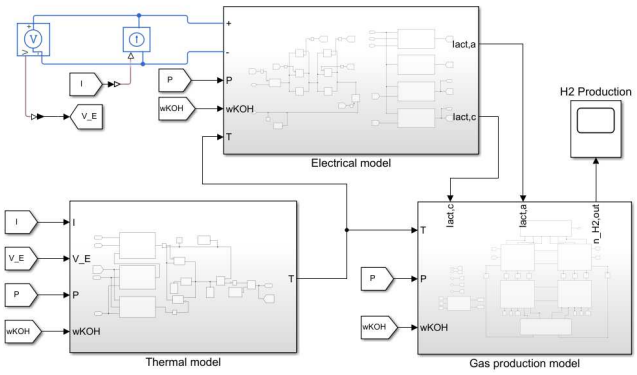

Fig. 3. Complete Simulink model of the AEC electrolyzer. It consists of three main interrelated modules: electrical, thermal and gas production.

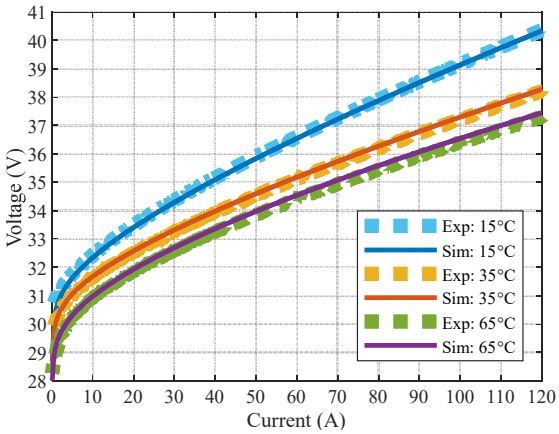

Fig. 4. Electrical model validation at static operation: experimental and simulated $I-V$ curves for temperatures of 15, 35 and 65 ºC, and a fixed operating pressure of 25 bar.

current values. This is because as temperature increases reversible voltage decreases, activation losses are reduced because electrochemical activity is favored, and ohmic losses also decrease due to an increase of electrolyte conductivity.

Second, the dynamic electrical response of the model has been assessed. This has been done by analyzing the effect of supplying the electrolyzer with sinusoidal currents of different amplitudes and frequencies. Simulated results show again a good agreement with the experimental data, as it can be seen in Fig. 5, which compares measured and simulated voltages when the electrolyzer is fed with a DC current of 60 A and a superimposed sinusoidal current of amplitude equal to 60 A and two different frequencies (0.1 and 100 Hz). At low frequencies, such as 0.1 Hz, the dynamic electrical response is quite similar to the stationary $I-V$ curve because the current evolution is not fast enough to excite the dynamic phenomena of the double-layer formation. But if the frequency reaches sufficiently high levels, such as 100 Hz, the dynamic electrical behavior is clearly appreciated due to current deviations through the double-layer capacitors.

B. Thermal submodel validation

In order to test the accuracy of the lumped capacitance thermal model, heating-cooling experiments were performed on the electrolyzer. Experimental temperature values have been recorded by means of a Pt 100 probe which reads the temperature inside the stack at the hydrogen collector output, and they are compared with the simulated temperature values of the lumped thermal mass. Fig. 6 shows the evolution of the

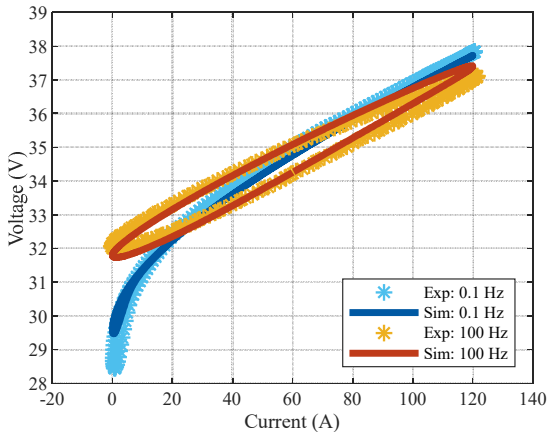

Fig. 5. Electrical model validation at dynamic operation: experimental and simulated voltage response to a sinusoidal input current $I = 60\left(1 + sin(2\pi ft)\right)$ (A). Operating conditions of 45 ºC and 25 bar.

experimental and simulated temperatures during a heating-cooling experiment in which the electrolyzer is fed with a DC current of 80 A for the first 12 hours, and then allowed to cool down by ambient air at 15 ºC for another 12 hours after switching off the input current, with the operating pressure fixed at 25 bar. As it can be seen, the model can predict the electrolyzer temperature with acceptable accuracy despite its simplicity.

C. *Gas production submodel validation*

Hydrogen production is the main function of water electrolyzers, so validating the model's ability to accurately predict hydrogen production rates at different currents, temperatures and pressures is essential. Furthermore, gas purity is another important issue that the model should be able to estimate with enough precision, especially because the lower operating limit of alkaline electrolyzers is mainly restricted by the anodic hydrogen content (HTO), which is usually greater than the OTH, in order to prevent the formation of explosive H_2 and O_2 mixtures [9].

Fig. 7 shows the experimental and simulated HTO values for different pressure and current levels, at a fixed operating temperature of 65 ºC. Furthermore, a comparison between measured and simulated H_2 output flow rates is also included. Only values corresponding to an operating pressure of 15 bar are represented in this case, as variations in the hydrogen production with pressure are negligible. As it can be seen, HTO increases with increasing pressure, which is associated to an increase in H_2 solubility in the electrolyte. Also, the linear relationship between the produced H_2 flow and electrical current can be clearly observed, as well as the reduction in gas impurities with higher current values. Simulated results for H_2 flow rates are slightly greater than the experimental data, which can be explained because the model is not considering hydrogen losses associated to the water supply system (the actual electrolyzer used in this study uses hydrogen for water supply pressurization) and control of electrolyte levels, but the accuracy of this gas production submodel has found to be quite satisfactory overall.

VI. Conclusions

In this contribution, a complete model for pressurized alkaline water electrolysis systems has been developed following a multiphysics approach. The model was developed using MATLAB/Simulink and validated with empirical data from a 1 Nm^3h^{-1} commercial electrolyzer, obtaining very satisfactory results. The model integrates electrochemical, thermal and gas production submodels, and is able to faithfully reproduce the main static and dynamic phenomena

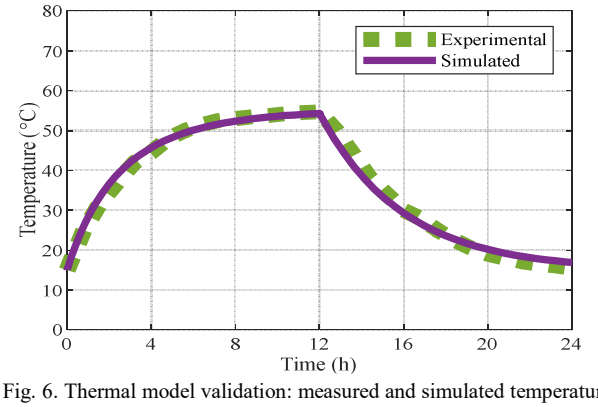

Fig. 6. Thermal model validation: measured and simulated temperature evolution of the stack fed with 80 A DC current and posterior cooling.

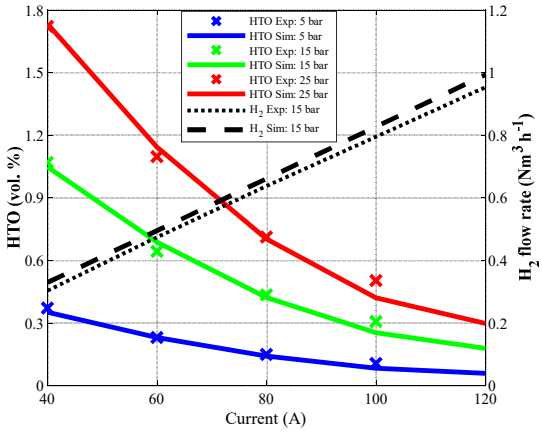

Fig. 7. Gas production model validation: HTO and H_2 production rates as a function of input current, at different operating pressures and a fixed temperature of 65 ºC.

that occurs in the electrolysis system. As it has been analyzed, operating conditions of temperature and pressure have an impact over the electrical consumption and the purity of the generated gases, aspects that could be critical for the operation of the electrolyzer coupled with renewable energies. Therefore, this model is appropriate due to its ability to reproduce the relationships between the different processes that take place inside the electrolyzer.

References

[1] S. A. Grigoriev, V. N. Fateev, D. G. Bessarabov, and P. Millet, "Current status, research trends, and challenges in water electrolysis science and technology," *Int. J. Hydrogen Energy*, vol. 45, no. 49, pp. 26036–26058, 2020, doi: 10.1016/j.ijhydene.2020.03.109.

[2] T. M. I. Mahlia, T. J. Saktisahdan, A. Jannifar, M. H. Hasan, and H. S. C. Matseelar, "A review of available methods and development on energy storage; Technology update," *Renew. Sustain. Energy Rev.*, vol. 33, pp. 532–545, 2014, doi: 10.1016/j.rser.2014.01.068.

[3] S. Sharma and S. K. Ghoshal, "Hydrogen the future transportation fuel: From production to applications," *Renew. Sustain. Energy Rev.*, vol. 43, pp. 1151–1158, 2015, doi: 10.1016/j.rser.2014.11.093.

[4] M. David, C. Ocampo-Martínez, and R. Sánchez-Peña, "Advances in alkaline water electrolyzers: A review," *J. Energy Storage*, vol. 23, no. April, pp. 392–403, 2019, doi: 10.1016/j.est.2019.03.001.

[5] O. Schmidt, A. Gambhir, I. Staffell, A. Hawkes, J. Nelson, and S. Few, "Future cost and performance of water electrolysis: An expert elicitation study," *Int. J. Hydrogen Energy*, vol. 42, no. 52, pp. 30470–30492, 2017, doi: 10.1016/j.ijhydene.2017.10.045.

[6] Ø. Ulleberg, "Modeling of advanced alkaline electrolyzers a system simulation approach," *Int. J. Hydrogen Energy*, vol. 28, pp. 21–33, 2003, doi: 10.1016/S0360-3199(02)00033-2.

[7] A. Ursúa and P. Sanchis, "Static-dynamic modelling of the electrical behaviour of a commercial advanced alkaline water electrolyser," *Int. J. Hydrogen Energy*, vol. 37, no. 24, pp. 18598–18614, 2012, doi: 10.1016/j.ijhydene.2012.09.125.

[8] P. M. Diéguez, A. Ursúa, P. Sanchis, C. Sopena, E. Guelbenzu, and L. M. Gandía, "Thermal performance of a commercial alkaline water electrolyzer: Experimental study and mathematical modeling," *Int. J. Hydrogen Energy*, vol. 33, no. 24, pp. 7338–7354, 2008, doi: 10.1016/j.ijhydene.2008.09.051.

[9] P. Haug, B. Kreitz, M. Koj, and T. Turek, "Process modelling of an alkaline water electrolyzer," *Int. J. Hydrogen Energy*, vol. 42, no. 24, pp. 15689–15707, 2017, doi: 10.1016/j.ijhydene.2017.05.031.

[10] A. Ursúa, P. Sanchis, and L. M. Gandia, "Hydrogen Production from Water Electrolysis : Current Status and Future Trends," *Proc. IEEE*, vol. 100, no. 2, pp. 410–426, 2012.

[11] M. Schalenbach, W. Lueke, and D. Stolten, "Hydrogen Diffusivity and Electrolyte Permeability of the Zirfon PERL Separator for Alkaline Water Electrolysis," *J. Electrochem. Soc.*, vol. 163, no. 14, pp. F1480–F1488, 2016, doi: 10.1149/2.1251613jes.